JHEP PROCEEDINGS *International Workshop on Astroparticle and High Energy Physics*

Experiments with Reactor anti-Neutrinos

Andreas Piepke*

Department of Physics and Astronomy
University of Alabama
Tuscaloosa, AL 35487
USA
E-mail: andreas@bama.ua.edu

Abstract: Disappearance oscillation searches at nuclear reactors are well suited for the exploration of large neutrino mixing. This paper summarizes the status of oscillation experiments making use of these low energy anti-neutrino sources.

1. Introduction

Experiments with reactor anti-neutrinos are and have been an essential tool for the understanding of neutrino oscillations at large mixing. After the original experimental proof of the existence of neutrinos by Reines and Cowan [1, 2], done at a nuclear reactor, reactor anti-neutrino experiments have been performed at ever increasing distance to the source in order to probe the mass composition of electron neutrinos, at smaller and smaller mass splittings. This paper will concentrate on recent oscillation studies. Reactors have also been used to study the magnetic moment of anti-neutrinos [3, 4] and to search for $\overline{\nu}_e$-decay [5]. These experiments will not be discussed.

Reactor anti-neutrinos are emitted during the beta-decay of a great variety of unstable fission fragments. Their energy distribution is thus continuous with a typical mean of $\langle E_\nu \rangle \approx 4$ MeV. Inverse beta decay (typically used to capture $\overline{\nu}_e$) cross sections are with $6 \cdot 10^{-43}$ cm^{-2}/fission extremely small. However, the anti-neutrino luminosity of a nuclear power reactor is very large thus partially offsetting this disadvantage.

After the experimental demonstration of large mixing in the neutrino sector the study of $\overline{\nu}_e$-disappearance at reactors is very much an up-to-date tool to further understand neutrino oscillations in both the solar and atmospheric Δm^2-range. The direct comparison of disappearance type experiments using particles and anti-particles requires conservation of CPT. In the following it is assumed that CPT is conserved. The recent observation of an event deficit by the KamLAND experiment [6] is a good example for the complementarity

*Speaker.

of reactor experiments. This measurement in fact provided totally solar model independent evidence for oscillations at the solar mass splitting and firmly established the Large Mixing Angle Solution of the solar neutrino problem. Both the CHOOZ [7] and Palo Verde [8] experiments, performed at 1 km distance to reactors, did not observe oscillations, resulting in a tight bound on the coupling of electron anti-neutrinos to the third mass eigenstate. A new generation of experiments at 1-2 km is now in the planning stage. Disappearance studies at rectors can thus constrain all mixing angles involved with electron neutrinos.
In disappearance searches the observable is the survival probability, P_{ee}. For three flavors it is given by:

$$\begin{aligned} P_{ee} = 1 - 4 \Big[& U_{e1}^2 \cdot U_{e2}^2 \cdot \sin^2 \frac{1.27\ \Delta m_{21}^2\ L}{E_\nu} + \\ & U_{e1}^2 \cdot U_{e3}^2 \cdot \sin^2 \frac{1.27\ \Delta m_{31}^2\ L}{E_\nu} + \\ & U_{e2}^2 \cdot U_{e3}^2 \cdot \sin^2 \frac{1.27\ \Delta m_{32}^2\ L}{E_\nu} \Big], \end{aligned} \tag{1.1}$$

where U_{ei} denotes the mixing amplitude of the electron neutrino with mass eigenstate i, $\Delta m_{ij}^2 \equiv m_i^2 - m_j^2$ (eV^2) the quadratic mass difference between mass eigenstates i and j, L (m) the distance between source and detector and, finally, E_ν (MeV) the neutrino energy. At reactors oscillations become evident by (a) comparing measured and expected reaction yield, and (b) by testing for spectral deformations introduced by the neutrino energy dependence of P_{ee}. The relatively low anti-neutrino energy allows testing of oscillations at both the solar and atmospheric mass splitting at relatively modest distances of 100 km and 1-2 km, respectively.
In the following the neutrino mixing matrix, commonly referred to as the Maki-Nakagawa-Sakata (MNS) matrix, is parametrized utilizing three rotational angles, θ_{12}, θ_{13} and θ_{23}:

$$U = \begin{pmatrix} c_{12}c_{13} & s_{12}c_{13} & s_{13} \\ -s_{12}c_{23} - c_{12}s_{23}s_{13} & c_{12}c_{23} - s_{12}s_{23}s_{13} & s_{23}c_{13} \\ s_{12}s_{23} - c_{12}c_{23}s_{13} & -c_{12}s_{23} - s_{12}c_{23}s_{13} & c_{23}c_{13} \end{pmatrix}, \tag{1.2}$$

where $c_{ij} \equiv \cos\theta_{ij}$ and $s_{ij} \equiv \sin\theta_{ij}$. The CP-violating phase has been dropped as it does not have observable consequence in disappearance experiments, discussed in this paper.

2. Oscillations at the Solar Splitting

A full three flavor analysis of current oscillation experiments [9] yields hierarchical mass splittings: $6.9 \cdot 10^{-5}$ eV^2 $= \Delta m^2_{\rm solar} \equiv \Delta m^2_{21} \ll 2.6 \cdot 10^{-3}$ eV^2 $= \Delta m^2_{\rm atm} \equiv \Delta m^2_{31}$. We can thus conclude that $\Delta m_{31}^2 \approx \Delta m_{32}^2$. An oscillation experiment utilizing reactor $\overline{\nu}_e$, sensitive to the solar mass splitting, has to be done at a distance $L_s \approx 100$ km so one argument of the oscillatory functions 1.1 approaches $\frac{\pi}{2}$. Under this condition the other two oscillatory functions will have a large argument, resulting in averaging: $\sin^2 \frac{1.27\ \Delta m_{31}^2\ L_s}{E_\nu} \approx$

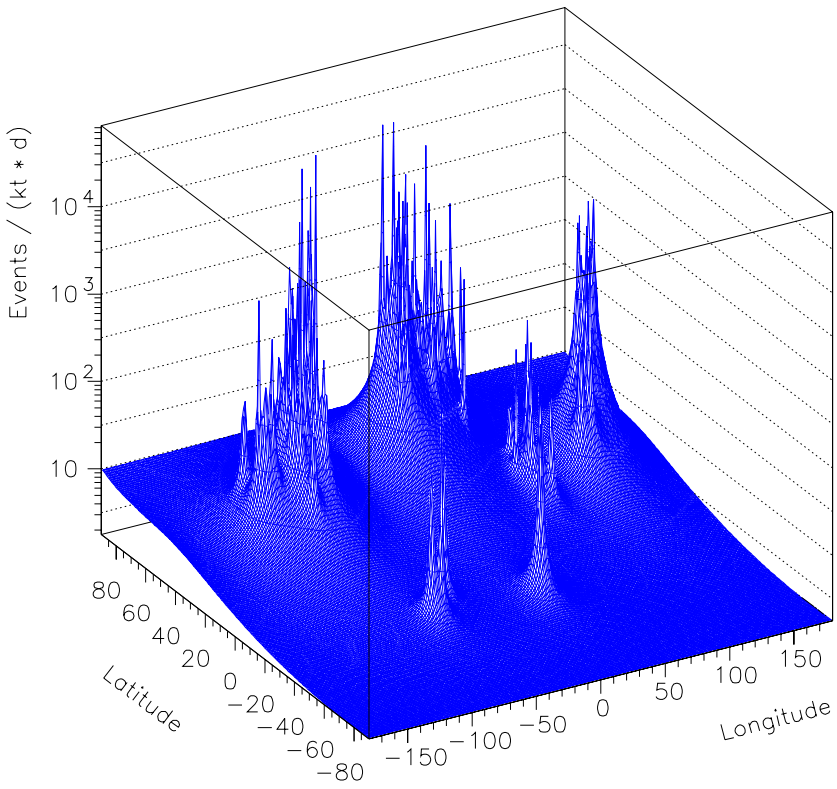

Figure 1: Inverse beta decay anti-neutrino interaction rate per unit time and mass as a function of longitude and latitude.

$\sin^2 \frac{1.27\ \Delta m^2_{32}\ L_s}{E_\nu} \approx \frac{1}{2}$:

$$P_{ee} \approx \underbrace{\cos^4\theta_{13}}_{>0.93}\left(1-\sin^2 2\theta_{12}\ \sin^2\frac{1.27\ \Delta m^2_{21}\ L_s}{E_\nu}\right) + \underbrace{\sin^4\theta_{13}}_{<1.2\cdot 10^{-3}}. \qquad (2.1)$$

The constraint on θ_{13} was again taken form ref. [9]. It is mainly determined by reactor oscillation searches at 1 km baseline [7, 8]. The apparent smallness of θ_{13} thus allows for a rather clean effective two flavor measurement of θ_{solar} and Δm^2_{solar} when using reactors at a large enough distance.

2.1 KamLAND

In order to measure $\overline{\nu}_e$-oscillations in the solar parameter range the source-to-detector distance has to be of order ∼100 km. This very large distance requires to either build an enormously large detector or find a site with many nuclear power reactors at the right distance. The site has to be underground to reduce background, a crucial requirement in

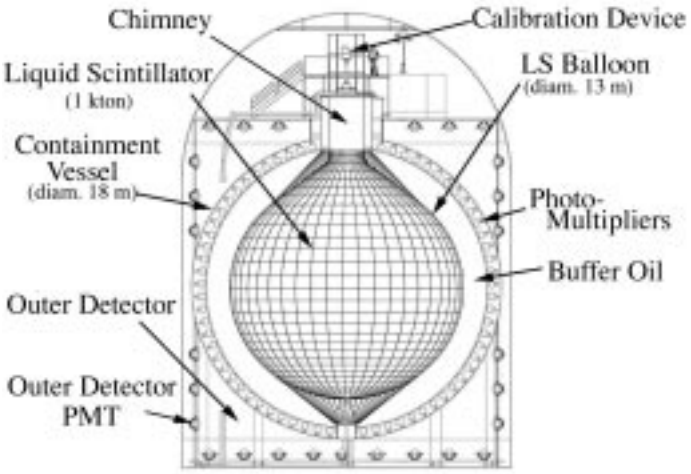

Figure 2: Schematic drawing of the KamLAND detector, taken from reference [6].

such a low energy and low rate experiment. Figure 1 depicts a model of the worldwide $\overline{\nu}_e$-interaction rate as a function of longitude and latitude. Such experiment is thus feasible only in North-America, Europe, or Japan.
The right combination of conditions is met in Kamioka, Japan. Here 54 powerful nuclear generating stations provide sufficient flux. Moreover 26 of them, responsible for 79% of the flux, are arranged at distances between 138-214 km, thus providing a well defined baseline. Kamioka is therefore an ideal site for such project.

The KamLAND experiment has been set up at the site of the concluded Kamiokande experiment in Kamioka, Japan to take advantage of this situation [6]. It consist of 1000 tons active target material, made of proton rich liquid scintillator. Inverse beta decay is utilized as detection reaction:

$$\overline{\nu}_e \; + \; p \quad \longrightarrow \quad e^+ \; + \; n \tag{2.2}$$

$$n \; + \; p \; \stackrel{\tau=200\mu s}{\longrightarrow} \; d \; + \; \gamma \; (2.2 \; MeV) \tag{2.3}$$

A temporal and spatial coincidence scheme is used to identify correlated inverse beta decay events. This greatly reduces random backgrounds, a big concern in low energy experiments. The tight time correlation between the prompt 2.2 and delayed 2.3 sub-events is central. Good spatial event reconstruction is equally important. The measurement of the energy of the reaction positron allows to determine the $\overline{\nu}_e$-energy, thus allowing to probe for spectral deformation as oscillation signature. The visible prompt energy, $\mathrm{E_{pr}}$, deposited into the scintillator after reaction 2.2, corresponds to the kinetic energy of the reaction positron plus twice its rest energy:

$$E_{pr} \; = \; E_\nu \; - \; \langle E_n \rangle \; - \; 0.8 \; \mathrm{MeV}, \tag{2.4}$$

where E_ν denotes the anti-neutrino energy, and $\langle E_n \rangle$ the average neutron recoil energy. Due to the large mass difference between neutron and positron $\langle E_n \rangle$ is between few tens to few hundred keV.

Figure 2 shows a cross sectional view of the detector. The detection medium is contained in a 135 μm thick, 13 m diameter balloon, suspended by ropes in a non-scintillating isoparaffin/dodecane buffer, acting as a transparent radiation shield. The fluids are contained in a spherical 18 m diameter stainless steel tank. 1879 PMTs, attached to its inner surface, are used for light read-out. 1325 PMTs are of a newly developed fast 17" type, while the balance is supplied by 20" PMTs, recovered from the Kamiokande experiment. Total photo cathode coverage is 34%, while the fast 17" PMTs alone account for 22% coverage. The detector has with $7.5\%/\sqrt{E\ (MeV)}$ an excellent energy resolution, with read-out of the 17" PMTs alone. The outer cylindrical volume is filled with 3.2 ktons of water and instrumented by 225 20" PMTs. It acts as a cosmic ray μ-veto and passive shield.
The bulk of the signal is provided by $\overline{\nu}_e$ emitted after fission of ^{235}U, ^{239}Pu, ^{238}U, and ^{241}Pu. The resulting $\overline{\nu}_e$-energy distributions have different hardness. The fuel composition in the cores of the reactors is evolving in time as a result of nuclear burn-up. A precise modeling of the interaction rates thus requires knowledge of the reactor power, to determine the overall flux, and the fuel composition. Such detailed information is available for all Japanese reactors based on an agreement between the KamLAND collaboration and the Japanese nuclear power reactor operators.
The cross section of detection reaction 2.2 is well understood, no nuclear matrix element is needed [10]. Using this input data, together with the known geographical locations of all power stations and the detector, the KamLAND collaboration can compute an expected reaction yield.

After 145.1 days of live time it was expected to observe $\mathrm{N_{NO}} = 86.8 \pm 5.6$ events, after cuts, in the absence of neutrino oscillations. The cuts include a rather restrictive energy threshold of 2.6 MeV, chosen to exclude any interference from anti-neutrinos emitted by natural radioactivity, the so-called geo-neutrinos. The efficiency of the cuts is with $(78.8 \pm 1.6)\%$ relatively large. The error given with the expected event yield reflects the sum of all systematic uncertainties. A fiducial volume cut provides the leading contribution. It can thus be expected that the systematic error will go down as the KamLAND collaboration improves their understanding of the detector. The $\overline{\nu}_e$-signal is expected to be superimposed to a background of $\mathrm{N_{BG}} = 1 \pm 1$ events. The effective Th and U concentrations of the scintillator are with $(5.2 \pm 0.8) \times 10^{-17}$ g/g and $(3.5 \pm 0.5) \times 10^{-18}$ g/g at unprecedented levels.

The observed number of events, again after cuts, was with $\mathrm{N_{Obs}} = 54$ events significantly lower than the no-oscillation expectation. The result has been reported as a ratio of observed over expected events:

$$\mathrm{R} \;=\; \frac{\mathrm{N_{Obs}} - \mathrm{N_{BG}}}{\mathrm{N_{NO}}} \;=\; 0.611 \pm 0.085^{\mathrm{stat}} \pm 0.041^{\mathrm{syst}}. \qquad (2.5)$$

The probability that the observed low event yield is due to a statistical fluctuation is $<0.05\%$.
The observation of a rate suppression at 138 to 214 km distance constitutes strong evidence that the Large Mixing Angle Solution is realized. All other potential solutions of the solar neutrino problem should not have resulted in a rate suppression. They are thus excluded

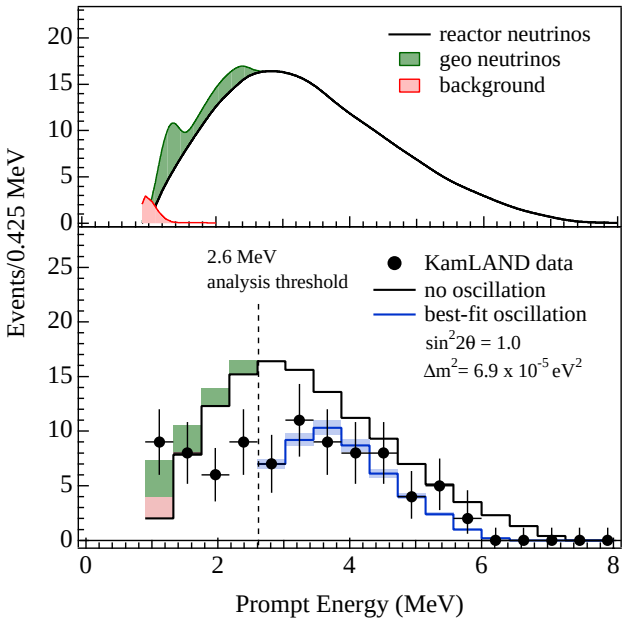

Figure 3: Energy distribution of prompt sub-events. The upper panel shows the expected distribution in the absence of oscillations, along with the backgrounds and geological $\overline{\nu}_e$-events. The solid circles with error bars in the lower panel depict the observed data set. The black histogram represents the no-oscillation spectrum, while the blue histogram shows the best fit. The shaded area indicates the systematic uncertainty. The estimated background is also indicated in the lower panel. This figure has been taken from reference [6].

at the confidence level given before.

For the appropriate combinations of Δm^2 and $\sin^2 2\theta$ neutrino oscillations should result in characteristic modifications of the prompt event spectrum. Figure 3 depicts the distribution observed after 145.1 days of live time in KamLAND. A spectral fit to the observed distribution favors an oscillation solution. However, a scaled non-deformed spectrum still results in an acceptable fit. More data is needed to better understand the event spectrum. The oscillation analysis performed by the KamLAND collaboration is summarized in a two dimensional $\sin^2 2\theta$-Δm^2 plot shown in figure 4. The observed rate deficit has been used to formulate an *exclusion* plot. All parameter combinations to the left of the solid line are excluded. This rules out all but the LMA. The spectral analysis results in a series of disconnected allowed islands. Due to the limited statistics the analytic power is still limited. However, there is overlap with the LMA solution, also shown in figure 4. The parameter range is further bracketed from above by data from the CHOOZ and Palo Verde experiments [7, 8], defining an allowed island totally independent of any solar physics.

By the time of writing of this article the KamLAND collaboration has increased its data set by a factor of more than 2.5.

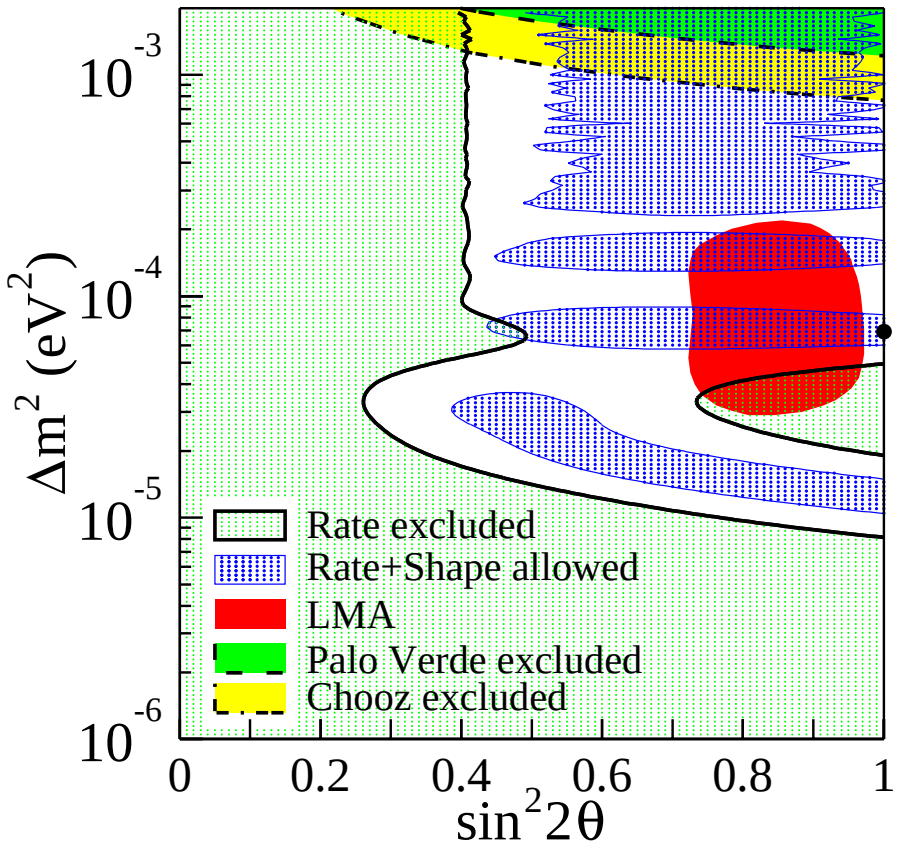

Figure 4: Parameters to the left of the solid black line are excluded by the rate analysis. This rather robust analysis is incompatible with all but the LMA solution of the solar neutrino problem (assuming CPT invariance) whose 95% c.l. contour is indicated too. The exclusions derived from the CHOOZ and Palo Verde experiments are indicated as dash-dotted and dashed lines, respectively. A combined rate and shape analysis yields a series of disconnected islands, allowed at 95% c.l.. The best fit to the data is indicated by black dot.

3. Oscillations at the Atmospheric Splitting

The three flavor analysis in reference [9] gives the following best fit for atmospheric neutrino oscillations: $2.6 \cdot 10^{-3}$ eV^2 $= \Delta m^2_{31}$. At a distance of $L_A = 1 - 2$ km: $\sin^2 \frac{1.27\ \Delta m^2_{21}\ L_A}{E_\nu} \approx 5 \cdot 10^{-4}$. Because of the hierarchical splitting we find: $\sin^2 \frac{1.27\ \Delta m^2_{31}\ L_A}{E_\nu} \approx \sin^2 \frac{1.27\ \Delta m^2_{32}\ L_A}{E_\nu}$. Using this approximation equation 1.1 can be simplified. A reactor disappearance experiment, set up at a distance L_A, thus determines P_{ee} to good approximation as:

$$P_{ee} \approx 1 - \sin^2 2\theta_{13}\ \sin^2 \frac{1.27\ \Delta m^2_{13}\ L_A}{E_\nu} - \underbrace{\cos^4 \theta_{13}\ \sin^2 2\theta_{12}\ \sin^2 \frac{1.27\ \Delta m^2_{21}\ L_A}{E_\nu}}_{very\ small\ at\ L_A \ll 10\ km}. \quad (3.1)$$

A reactor disappearance search at such a shorter baseline provides a rather clean measurement of θ_{13}, the last truly unknown mixing matrix element. The interference with the solar splitting is very small. To good approximation one is dealing with two flavor oscillations.

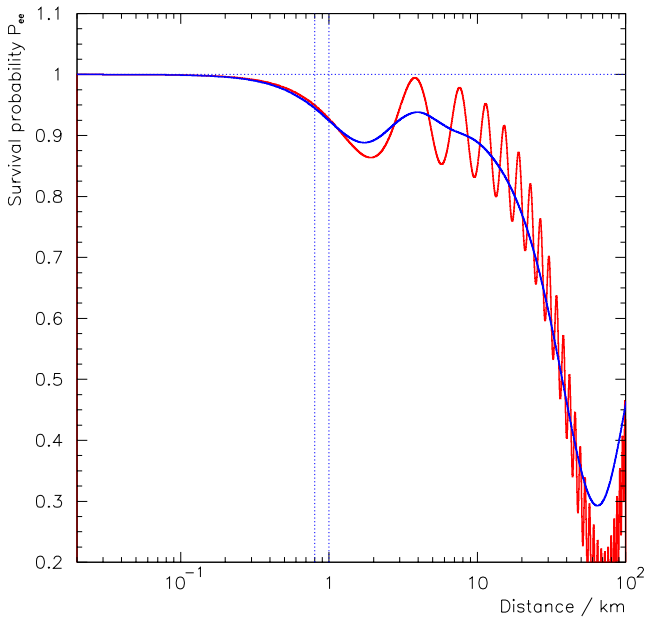

Figure 5: Electron neutrino survival probability as a function of distance. The strongly oscillating curve has been calculated using equation 3.1 and a fixed average neutrino energy of 4 MeV. The smooth curve was calculated as the ratio of the interaction rate with and without oscillations defined in equation 3.2. The two vertical lines indicate the positions of two concluded oscillation experiments at the CHOOZ and Palo Verde nuclear generating stations. The best fit solar and atmospheric parameters and the 2σ limit for θ_{13}, as given in [9], have been used for this plot.

Figure 5 shows P_{ee} calculated using equation 3.1 as a function of distance to the reactor. The strongly oscillating curve was calculated using equation 3.1 directly assuming an average anti-neutrino energy of $\mathrm{E}_\nu = \langle \mathrm{E}_\nu \rangle = 4$ MeV. The rapid shallow minima are due to θ_{13}. The current best limit has been used in this calculation [9]. As discussed above the reactor anti-neutrino spectrum is continuous. Experiments testing total interaction rates are thus averaging over both the anti-neutrino spectra and the interaction cross section. In order to better understand the effect of this averaging a modified survival probability, $\langle P_{ee} \rangle$, is defined:

$$\langle P_{ee} \rangle \;=\; \frac{\sum_i \int_{E_{th}}^{E_{up}} \phi_i(E_\nu)\; \sigma(E_\nu)\; P_{ee}\; dE_\nu}{\sum_i \int_{E_{th}}^{E_{up}} \phi_i(E_\nu)\; \sigma(E_\nu)\; dE_\nu}, \tag{3.2}$$

where the sum goes over all fissile isotopes, i, $E_{th} = 1.8$ MeV denotes the reaction threshold, $E_{up} = 10$ MeV the upper energy cut-off, E_ν the anti-neutrino energy, $\phi_i(E_\nu)$ the anti-neutrino spectrum of fissile isotope i (taken from reference [11]), and $\sigma(E_\nu)$ the differential reaction cross section (taken from reference [10]). $\langle P_{ee} \rangle$ is an observable quantity. $\langle P_{ee} \rangle$, plotted as a function of distance is also shown in figure 5. The averaging washes out all but the first oscillation minimum, attributed to θ_{13}. It is expected to be located around 1.7 km. The deep minimum at about 100 km corresponds to the solar mass splitting and

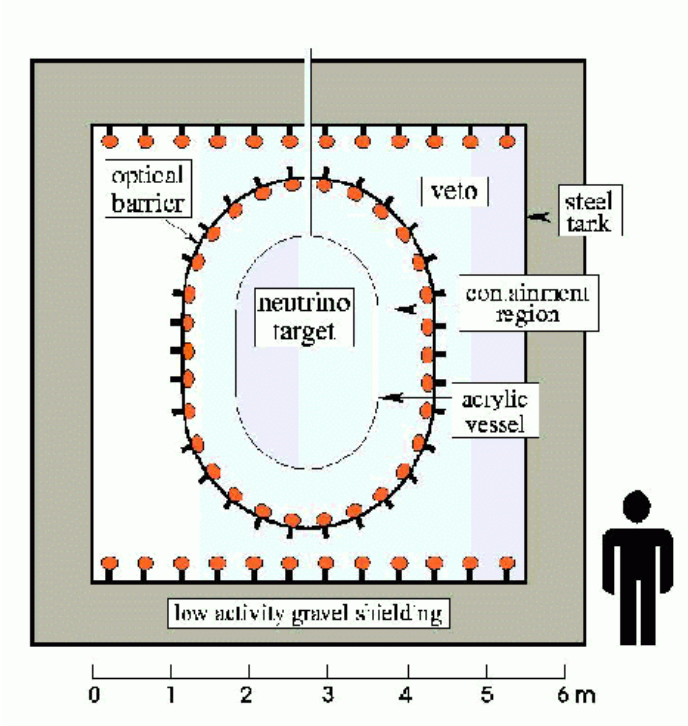

Figure 6: Schematic drawing of the CHOOZ detector, taken from reference [7].

mixing and is being explored by the KamLAND experiment, discussed before.
It has been pointed out in the literature [12] that the oscillation probability, $P_{\mu e}$, to be measured in off-axis accelerator experiments is subject to degeneracies. $P_{\mu e}$ depends besides θ_{13} also on the overall sign of Δm^2_{31} and is sensitive to CP effects. This situation can be resolved by running with both particle and anti-particle beams. A measurement of θ_{13} at a nuclear reactor would thus be an important complement to these accelerator projects, helping to lift degeneracies. If θ_{13} on the other hand cannot be measured a sufficiently tight bound may discourage very long baseline studies of CP-violation in the Lepton sector. CP-violating effects are proportional to $\sin\theta_{13}$ [13].

The existing limit on θ_{13} is mainly driven by reactor experiments performed at a baseline of about 1 km. However, the CHOOZ [7] and Palo Verde [8] experiments were initially not set up for this purpose. Main goal of both experiments was to investigate whether $\nu_\mu \rightarrow \nu_e$ oscillations are the leading cause of the atmospheric neutrino anomaly. Both experiments could conclusively rule out this possibility. Upon construction neither experiment had been optimized for to probe small admixtures. In the following both experiments are briefly discussed.

3.1 Chooz

From 1997 to 1998 a French-Italian-US collaboration operated a 5 ton anti-neutrino detec-

tor 1000 and 1100 m away from two nuclear generating stations, near Chooz (France) [7]. The detector, depicted in figure 6, was housed in an underground lab at an overburden of 300 mw.e.. Anti-neutrinos were detected using inverse beta decay, as described in equation 2.2. In contrast to the previously described KamLAND project this experiment made use of 0.1% Gd loaded scintillator. Gd has a large thermal neutron capture cross section and emits an 8 MeV gamma ray burst after capture:

$$\mathrm{n} \; + \; \mathrm{Gd} \; \stackrel{\tau=30\mu\mathrm{s}}{\longrightarrow} \; \mathrm{Gd}^{*} \; + \; \gamma(8\ \mathrm{MeV}). \tag{3.3}$$

Replacing the capture reaction defined in 2.3 by 3.3 results in a much shortened correlation time between prompt and delayed sub-event and, as a further benefit, boosts the energy release after neutron capture above that of natural radioactivity. Such loading thus enhances robustness against random background.
The CHOOZ detector was composed of several layers. The inner anti-neutrino target consisted of the described 5 tons of Gd loaded scintillator, contained in an acrylic vessel. It was surrounded by a 70 cm thick layer of un-doped liquid scintillator. This zone served as a containment for the gamma radiation emitted after positron annihilation and by Gd after neutron capture. It helped create a clean Gaussian energy response, not affected by partial energy loss near the detector boundary. The next layer was made of 90 tons of mineral oil acting as an active radiation shield, housed in a steel tank. The two inner layers were viewed by 192 eight inch phototubes, mounted on a non-transparent support structure. The outer detector was instrumented with 24 8" PMTs. The experiment had an excellent energy resolution of $\sigma(\mathrm{E})/\mathrm{E} = 5.6$ % (at 8 MeV), at a photo cathode coverage of 15%. Event selection made use of the temporal and spatial correlation of the two sub-events. The combined efficiency of the cuts was estimated to be $(69.8 \pm 1.1)\%$. After application of the data selection cuts a signal-to-background ratio of 10:1 was achieved. The good overburden was an important factor in achieving this excellent duty factor. The background was directly measured during reactor-off periods.
The ratio of events with and without oscillations, as defined in equation 2.5, was reported as: $\mathrm{R} \; = 1.01 \pm 0.028^{\mathrm{stat}} \pm 0.027^{\mathrm{syst}}$. This consistency of observed and expected number of events, in absence of neutrino oscillations, was used to construct an excluded area in the Δm^2-$\sin^2 2\theta$ parameter space. The resulting 2-dimensional limit is shown in figure 8. It should also be noted that the reported R-value provides implicit proof that reactor anti-neutrino emission and detection are indeed well understood as advertised.

3.2 Palo Verde

From 1998 to 2000 this experiment was performed by a US collaboration at 750 and 890 m distance to the three reactors of the Palo Verde Nuclear Generating Station, the largest US nuclear plant [8]. The experiment was performed at the rather shallow depth of 32 mw.e.. The detector consisted of 11.3 tons of 0.1% Gd loaded liqiuid scintillator. A detector schematics is shown in figure 7. Unlike KamLAND and CHOOZ the detector was not homogeneous but consisted of 66 segments in form of 9 m long acrylic tanks, instrumented with 132 5" PMTs. Again inverse beta decay (equation 2.2) was utilized. The scintillator

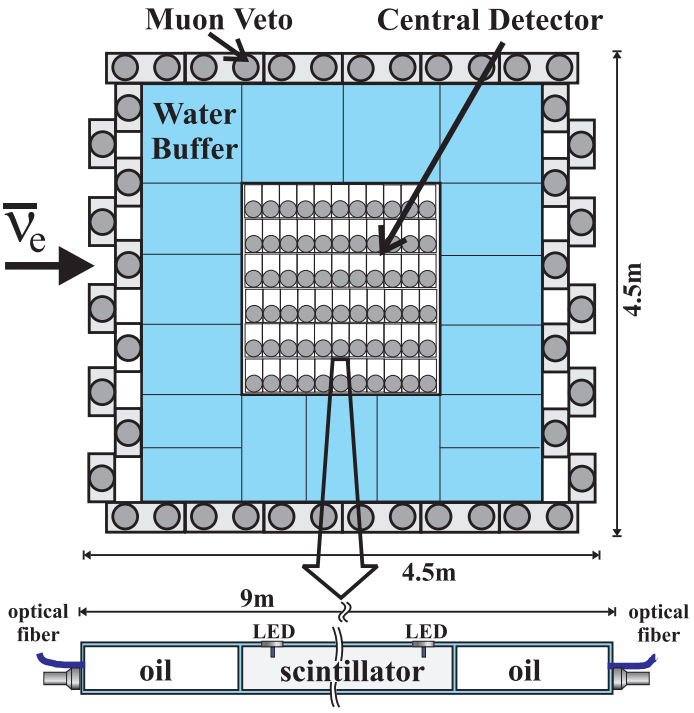

Figure 7: Schematic drawing of the Palo Verde detector, taken from reference [8].

segments were contained in a 1 m thick passive water shield. The water in turn was surrounded by a hermetic muon veto system, consisting of liquid scintillator contained in PVC tanks.

The segmentation allowed to tag events in a four fold coincidence scheme. The prompt part of a candidate event would be identified by requiring a fast triple coincidence. The energetic reaction positron of reaction 2.2 would fire one detector segment. After coming to rest it would annihilate. The segments were designed small enough as to allow the annihilation gammas to escape with a high probability. They would then fire at least two neighboring cells to complete the triple coincidence. The reaction neutron would thermalize and then capture on Gd, as described in 3.3. A delayed high energy deposit in the vicinity of the prompt event would constitute the fourth coincidence. Due its shallow overburden Palo Verde had to cope with a substantial neutron background. The four fold coincidence scheme made this manageable. However, even with this active background rejection capability the signal to background ration was 1:1.2, averaged over all full power periods. Background and anti-neutrino signal were determined in two different ways:

- The more conventional approach made use of periods of reduced anti-neutrino flux when one of the three reactors was down for refueling. The background could be inferred from the observed variation in the signal, compared to the expectation.

- The novel so called swap method made use of the apparent symmetry of several backgrounds under the exchange of the prompt and delayed sub-event selection criteria. These backgrounds thus largely cancel in the difference of the original and swapped

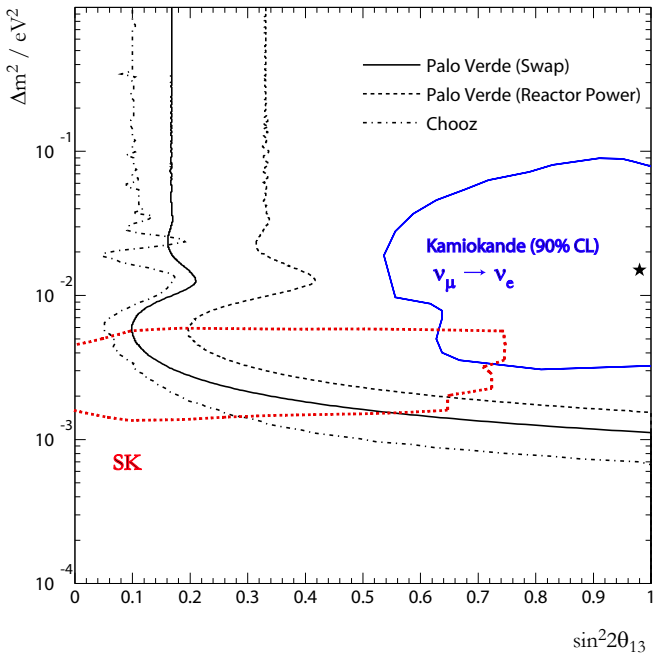

Figure 8: Neutrino parameters to the right of the lines labeled "Palo Verde" (solid) and "Chooz" (dash-dotted) are excluded at 90% c.l.. This figure has been taken from reference [8]. The $\sin^2 2\theta_{13}$-parameter range (inside the dotted red curve), allowed by a preliminary analysis of the Super-Kamiokande collaboration, has been superimposed. This curve has been taken from reference [14]. The solid (blue) line labeled "Kamiokande" represents the allowed parameter space for $\nu_\mu \to \nu_e$ as reported in [15].

rates. Only about 20% of the anti-neutrino signal cancels in this subtraction thus allowing a background determination independent of the reactor power schedule. Application of this method allowed a statistically more powerful oscillation search at the expense of a somewhat stronger reliance on Monte Carlo simulations, needed to quantify the extent of the signal cancellation and the magnitude of the remaining non-canceling background components.

The event selection efficiency, including all dead time corrections, was estimated as $(11.2 \pm 0.6)\%$. Both analysis' consistently found no evidence for neutrino oscillation. The ratio of events with and without oscillations, based on the "swap" analysis, was reported as: $\mathrm{R} = 1.01 \pm 0.024^{\mathrm{stat}} \pm 0.053^{\mathrm{syst}}$.

Besides the main goal of probing whether or not $\nu_\mu \to \nu_e$ oscillations are responsible for the atmospheric neutrino anomaly, the absence of oscillations involving electron neutrinos in the atmospheric Δm^2-range has been used to place a limit on $\sin^2 2\theta_{13}$. This bound is shown in figure 8 together with the allowed parameter range derived from the Super-Kamiokande experiment [16]. CHOOZ provided the more stringent constraint. While two mixing angles are found to be large the reactor experiments thus provide evidence that θ_{13}

has to be quite small.

3.3 New Projects

A new disappearance test with reactor anti-neutrinos at 1 to 2 km distance with 5 to 10 fold improved sensitivity compared to CHOOZ would provide important input for our understanding of neutrino mixing and for the planning of new large scale long baseline experiments.
The main question is how to achieve such improved sensitivity? In CHOOZ, which can serve as a bench-mark, statistics and systematic contributed to equal parts to the total error. Uncertainties in the reaction cross section and the reactor modeling were responsible for most of the systematic error. In order to cancel these uncertainties from the observed rate or spectral distribution, experiments with 2 or more detectors, sampling over the same beam at different distances, have been proposed [17]. If the detectors are identical, or their relative response is understood well enough, a comparison of the rates, taken at two distances would allow an oscillation test independent of the absolute $\overline{\nu}_e$-flux. The cancellation of the reactor physics could also be achieved by utilizing a movable detector. Reference [12] gives a detailed overview over the statistical considerations governing the planning of such project. Figure 9 illuminates how the spectral ratio can be utilized to determine the underlying neutrino parameters. Figure 9 shows the ratio of energy distributions taken at 0.5 km distance divided by that taken at 1.7 km distance, after solid angle correction. The black curve reflects the expected ratio if all relevant neutrino parameters are at their current best fit values, and θ_{13} is near its 2 σ limit. To obtain the red curve the atmospheric mass splitting was changed to $\Delta m^2_{\rm atm} = 2.0 \cdot 10^{-3}$ eV^2, resulting in a shift of the minimum to lower visible energies. Finally, the purple curve was calculated using $\sin^2 2\theta_{13} = 0.02$ while leaving all other neutrino parameters at their best fit values. The energy of the minimum thus determines $\Delta m^2_{\rm atm}$, the depth of it $\sin^2 2\theta_{13}$. To make use of this analytic power requires a low threshold detector, and well understood energy calibrations in both detectors. The test of a very small mixing angle is certainly a non-trivial technical challenge.
A variety of reactor experiments is under consideration. Various collaborations around the world are investigating experiments at the Chooz (France), Daya Baya (China), Diablo Canyon (USA), Kashiwazaki (Japan), Krasnoyarsk (Russia), Tihange (Brazil) and other sites. Their goal is to measure $\sin^2 2\theta_{13}$ down to the 0.01-0.02 level. In order to achieve such precision a deep underground site, at least for the far detector, is imperative. Again the CHOOZ experiment sets the scale. The unfolding of background for the different detectors might otherwise limit the sensitivity. The exploration of potential experimental sites has been guided by the topography of the site.
In order to collect sufficient statistic 50 to 100 ton detector sizes are being discussed for the far detector. All projects are considering to utilize inverse beta decay and organic liquid scintillator. Due to stringent requirements regarding time stability of the detector it is not yet clear whether or not Gd loading will offer a net advantage. However, it seems clear that a homogeneous detector design is superior, especially at a location with sufficient overburden.

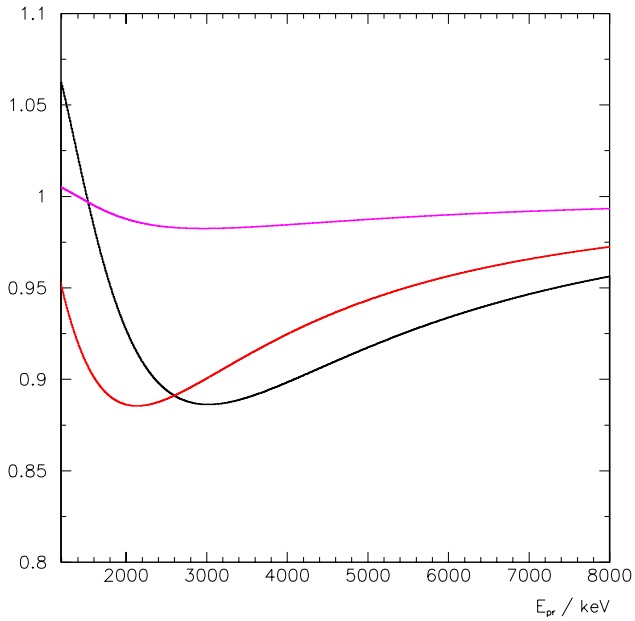

Figure 9: Ratio of energy distributions expected at 0.5 km over that at 1.7 km distance. The black curve has been calculated for $\Delta m^2_{\rm solar} = 6.9 \cdot 10^{-5}$ eV^2, $\sin^2 2\theta_{\rm solar} = 0.84$, $\Delta m^2_{\rm atm} = 2.6 \cdot 10^{-3}$ eV^2, and $\sin^2 2\theta_{13} = 0.135$, assuming that the quantity of interest is near its current 2 σ limit. A variation of $\Delta m^2_{\rm atm} = 2.0 \cdot 10^{-3}$ eV^2 results in the red curve. The purple curve was calculated using $\sin^2 2\theta_{13} = 0.02$ (all other parameters at their best fit values), a value close to the projected sensitivity of new experiments. All curves have been corrected for differences in solid angle. The distributions are determined as a function of the visible energy of the prompt sub-event, as defined in equation 2.4.

4. Conclusion

Experiments with reactor anti-neutrinos provide important and up to date constraints on the neutrino mass splittings and the mixing angles involving electron neutrinos. At the solar mass splitting the KamLAND experiment provided solar model independent evidence that neutrino oscillations are indeed causing the solar neutrino deficit, leaving very little room for alternate explanations. The CHOOZ and Palo Verde experiments showed that θ_{13}, unlike the other mixing angles, has to be small. A new generation of reactor experiments, to be performed at 1-2 km baseline, aims at an ambitious test of θ_{13}. This could be achieved at a fraction of the costs associated with most other approaches. These experiments are difficult but hold the promise to tell us more about θ_{13} within a few years.

References

[1] F. Reines and C.L. Cowan, *Phys. Rev.* **92** (1953) 830

[2] F. Reines et al., *Phys. Rev.* **117** (1960) 159

[3] Z. Daraktchieva et al., *Phys. Lett.* **B 564** (2003) 190

[4] H.B. Li, et al., *Phys. Rev. Lett.* **90** (2003) 131802

[5] L. Oberauer et al., *Phys. Lett.* **B 198** (1987) 113

[6] K. Eguchi et al., *Phys. Rev. Lett.* **90** (2003) 021802

[7] M. Apollonio et al., *Eur. Phys. J.* **C 27** (2003) 331

[8] F. Boehm et al., *Phys. Rev.* **D 64** (2001) 112001

[9] M. Maltoni et al., *Phys. Rev.* **D 68** (2003) 113010

[10] P. Vogel and J.F. Beacom, *Phys. Rev.* **D 60** (1999) 053003

[11] P. Vogel and J. Engel, *Phys. Rev.* **D 39** (1989) 3378

[12] P. Huber et al., *Nucl. Phys.* **B 665** (2003) 487

[13] D.V. Ahluwalia, Y. Liu, I. Stancu, *Mod. Phys. Lett.* **A 17** (2002) 13

[14] F. Boehm et al., *Phys. Rev.* **D 62** (2000) 072002

[15] Y. Fukuda et al., *Phys. Lett.* **B 335** (1994) 237

[16] K. Okamura, Ph.D. Thesis University of Tokyo, (1999)

[17] L. Mikaelyan, *Nucl. Phys.* **91** *(Proc. Suppl.)* (2001) 120